TIME-LAPSE SEISMIC DATA REGISTRATION AND INVERSION FOR CO_2 SEQUESTRATION STUDY AT CRANFIELD

Rui Zhang[1], Xiaolei Song[2], Sergey Fomel[2], Mrinal K. Sen[23], and Sanjay Srinivasan[2]

[1]*Lawrence Berkeley National Laboratory*
[2]*The University of Texas at Austin*
[3]*National Geophysical Research Institute, Hyderabad, India*

ABSTRACT

Time-lapse seismic survey for CO_2 sequestration study at Cranfield can be problematic because of misalignments between the time-lapse datasets. Such misalignments can be caused by any step of seismic data processing workflow, which may result in misunderstanding of time-lapse seismic amplitude differences. There are many matching processing methods under development, but these methods are still immature and very time consuming. We propose an efficient local-correlation based warping method to register the time-lapse post-stack datasets, which can align the time-lapse datasets without changing the original amplitudes. The application of the registration of Cranfield time-lapse datasets demonstrates its effectiveness in separating the time-shift character from the seismic amplitude signature. After registration, the time-lapse differences show improved consistence in vertical cross-sections and more localized distribution of the difference amplitudes in horizon slices, which allows us to apply a basis pursuit inversion for acoustic impedances. The inversion results show that decreases of acoustic impedances mostly occur at the top of the injection interval, which can be used as alternative rock properties to detect the subsurface CO_2 plume.

INTRODUCTION

Cranfield is an old oil field, which was first discovered in 1940's. The production decreased dramatically after 1960's (Mississippi Oil Gas Board, 1966). These early industry applications provided plentiful regional geology information and left lots of existing wells available for CO_2 injection. The Gulf Coast Carbon Center (GCCC) at the Bureau of Economic Geology started CO_2 injection in 2008 together with various studies and analysis utilizing different kinds of well-logging and seismic methods (Meckel and Hovorka, 2009). Although the well-logging measurements can provide direct in situ information in depth, they are spatially sparse. This necessitates use of time-lapse (4D) surface seismic measurements.

The time-lapse seismic datasets at Cranfield consist of two surveys one each during pre- and post- CO_2 injection. Pre-injection 3D seismic survey was acquired in 2007 before the first

injection in July 2008, which achieved injection rates greater than 1.2 million tonnes per year though 23 wells, with cumulative mass injected as of August, 2010 of 2.2 million metric tonnes, when the post-injection 3D seismic survey was acquired in September 2010. Injection is into coarse grained fluvial deposits of the Cretaceous lower Tuscaloosa Formation in a gentle anticline at depths of about 3000 m. Different kinds of in situ well-log measurements have been recorded during injection, such as well-bore temperature, pore pressure, confining pressure, reservoir saturation tool, etc., which enabled calibration with the time-lapse seismic survey (Klicman et al., 1988, Hovorka et al., 2011). From these measurements, we did not find any emission or leakage of the injected CO_2 above the injection interval.

The time-lapse seismic datasets are expected to capture the variation of subsurface rock properties, but the effective evaluation of subsurface fluid volumes and associated saturations from time-lapse seismic still remains a challenging task. Lumley (2001) summarizes most key points of successful time-lapse seismic monitoring including the critical reservoir rock and fluid properties, pressure and temperature values, and high-fidelity seismic acquisition, processing, and interpretation. Because of relatively small rock properties change induced by fluid flow, Calvert (2005) attributes the future of 4D seismic technology to enhancing sensitivity of seismic data to such small changes. MacBeth et al. (2006) and Falahat et al. (2011) attempt to calibrate production data with time-lapse seismic data by flow simulation methods to provide quantitative evaluation of the reservoir. Landrø (2002) provides an uncertainty analysis of time-lapse seismic for fluid properties estimation. Worldwide case studies of time-lapse seismic applications on various rock types demonstrate the feasibility of this technique and its potential for quantitative reservoir characterization (Burkhart et al., 2000; Reid et al., 2005; Staples et al., 2005; Isaac and Lawton, 2006; Wagner et al., 2006; Hall et al., 2006; Vedanti and Sen, 2009).

Various techniques have been developed for time-lapse seismic applications (Rickett and Lumley, 2001). Hall et al. (2005), Hall (2006), and Hale (2009) have introduced a local correlation based warping technique to detect the displacement between time-lapse datasets. An analogous local correlation based warping has later been used to register monitor and base survey (Fomel and Jin, 2009). The key difference between these applications lies in the understanding of the time-shifts of time-lapse seismic datasets. Either the time-shifts are considered as a real time-lapse signature caused by production or fluid movements, or they are considered as an aliasing induced by data acquisition or processing. In the case of Cranfield datasets, we attribute the time shifts to the latter. The first reason for this recognition lies in the evidence that there is no emission or leakage of injected CO_2 found at overburden layer with current well-log measurements. The second reason is the thin-bed characteristic of the injection interval and the small change of velocity could be caused by the injected CO_2. To verify this recognition, we compute the local time shift between the time-lapse seismic datasets at Cranfield,

showing nearly constant time shifts from the shallow to the deep formation beneath the injection interval. In addition, the lateral change of the time shifts shows somehow correlation with the polarity change of difference amplitude within the injection interval, which will be presented later. Thus, we consider the time-shift between time-lapse datasets at Cranfield as an aliasing, but the seismic amplitude change can reflect fluid properties change, which lead to seismic inversion for time-lapse rock properties changes. Seismic inversion, as the commonly used techniques for reservoir characterization, is applied on time-lapse datasets for detection of changes in reservoir properties (Buland and Ouair, 2006; Vedanti and Sen, 2009).

In this paper, the registration of time-lapse datasets is accomplished by warping the post-injection to the pre-injection datasets based on the local-correlation between them. The derivation of the local-correlation is using normalized amplitudes, while the warping is applied on the original amplitudes. In this way, the time-shift effect can be separated from the amplitude changes. After the registration, we invert the time-lapse datasets into the subsurface acoustic impedances with a basis pursuit inversion (Zhang and Castagna, 2011). The basis pursuit inversion (BPI) utilizes L1-norm optimization with incorporation of a wedge dictionary to approach high resolution. Such time-lapse impedances and their difference are integrated with other information for effective mapping of the CO_2 movements.

GEOLOGY OF CRANFIELD AND DATA PREPARATION

The updip lower Tuscaloosa trend of southwest Mississippi occurs along the southern rim of the Mississippi Salt Basin. The lower Tusaloosa Formulation is found here at subsea depths of about 3000 to 4200 meters (Hersch, 1987) along gentle regional dip to the southwest. First generation fields within this part of trend (e.g, Cranfield, Brookhaven, Mallalieu, and Baxterville), discovered in the 1940's, are anticlinal and fault closures related to deep salt structures (Womack, 1950). The injection interval at the Cranfield is located at southwest Mississippi (Figure 1 (a)), at the lower Tuscaloosa Formation from 3012 to 3142 meters below surface. It is a near circular anticline about 6.4 km in diameter from the original full coverage 3D seismic survey, as shown in Figure 1 (b). The dip of the formation ranges from 1 to 3 degrees. A major NW-SE directional fault, which is sealing, except in the north part of the field, divides the productive formation into two reservoirs. The time-lapse seismic survey for CO_2 sequestration study was focused on the northeast part of the anticline, as shown in the yellow area in the Figure 1 (c). Twenty three existing wells, labeled as red triangles, have been used for CO_2 injection. Two-way-travel (TWT) time has been mapped at the top of lower Tuscaloosa Formation, showing the center of anticline at the lower left corner of Figure 1 (d).
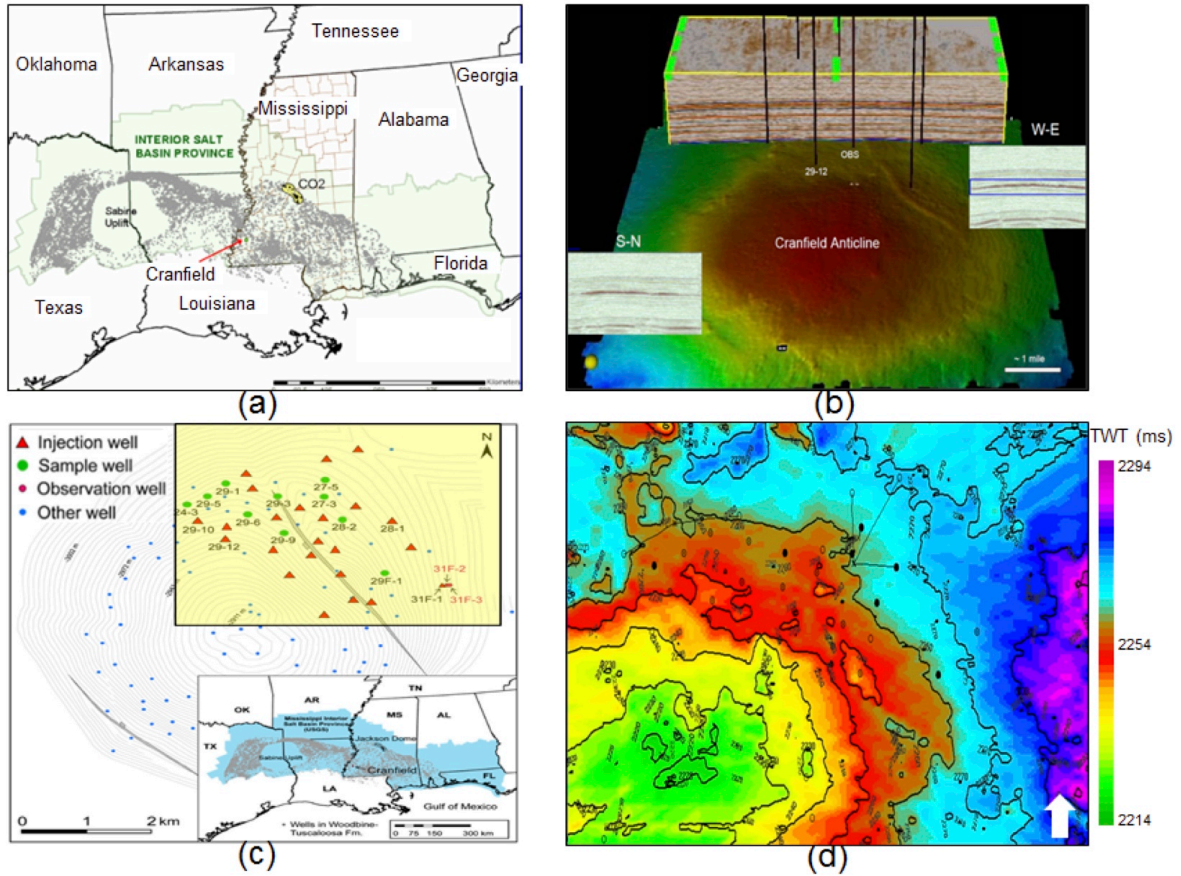
Figure 1. Overview of Cranfield. (a) map location of Cranfield; (b) the surface and lower Tuscaloosa formation; (c) original 3D seismic data; (d) time-lapse seismic coverage (Zhang et al., 2012).

The Tuscaloosa Formation comprises the Basal Formation of Gulf series of Upper Cretaceous ages (Figure 2). The left panel of the Figure 2 shows the regional sequence stratigraphy and the upper right panel shows a geological cross-section with the Cranfield pointed out with the yellow circle. The lower right panel shows the zoomed view of the injection interval of the lower Tuscaloosa Formation. An unconformity separates the Basal Tuscaloosa from the older Washita Fredericksburg Formation of Lower Cretaceous ages. The sand has been described as having large amounts of chloritic materials and shaly in some areas. The Lower Tuscaloosa Formation has traditionally been divided into two members: a Basal Massive Sand Member and a conformably overlying Stringer Sand Member, with informal local and field designations given to individual sands within these members. Spooner (1964) referred to the Basal unit in northwest Louisiana as the Buckhorn sand, and believed it to be younger than the Massive Sand of Mississippi.
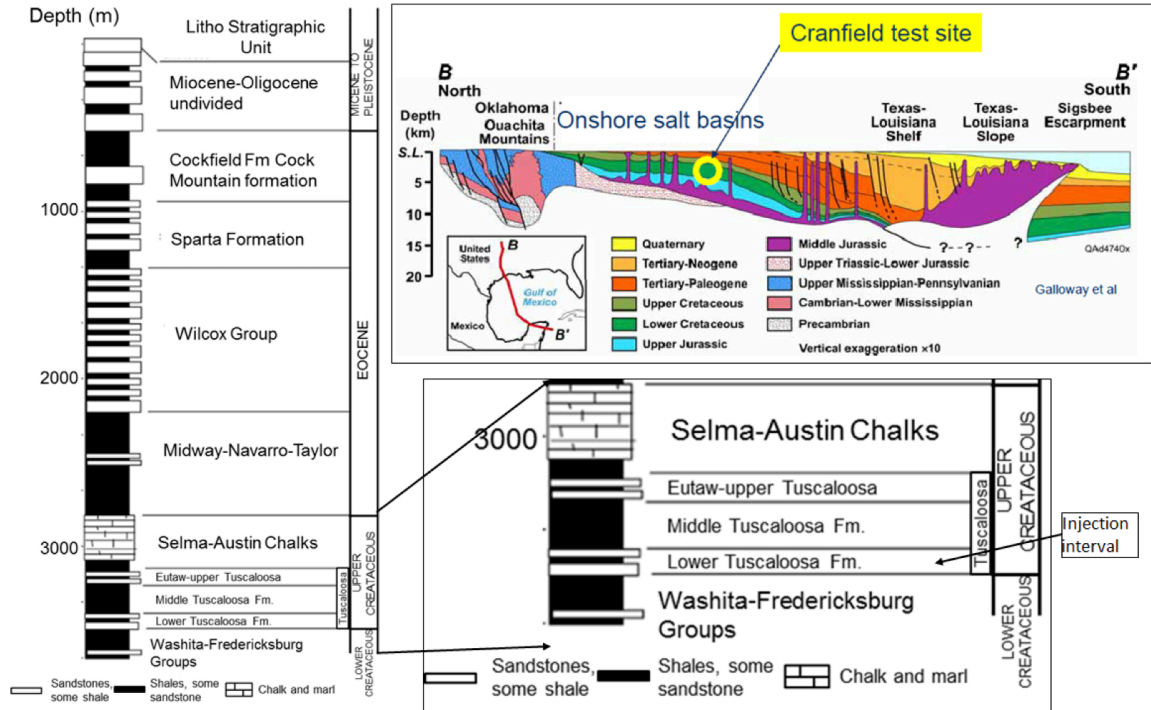
Figure 2. Stratigraphy and geological section (Zhang et al., 2012).

The cross-sections of the time-lapse datasets are shown in Figure 3. Figures 3 (a) and (b) show the pre- and post- injection data with the top and base of the injection interval mapped out, where the yellow zone in Figure 3 (a) represents the lower Tuscaloosa Formation for CO_2 injection. A single trace at the location marked by the dashed black line will be selected for 1D registration example later. A well located at the black triangle will be used for seismic well tie. The difference (Figure 3 (c)), which is calculated by subtracting the post- from pre- injection datasets, shows relatively strong amplitudes around the injection interval. Both two far ends of the sections in Figure 3, appearing noisier than the middle parts, are at the boundary of the surveys, which suffer from the lack of the data coverage or inaccurate velocity model for imaging. The time-lapse differences (Figure 3 (c)) within the injection interval appear as negative values at the middle part of the cross-section; and nearly zero values at the two near sides; but positive values at the far sides. We define the negative differences as blue color zone, nearly zero differences as green color zones and positive differences as orange color zones in Figure 3 (c). Landrø (2001) introduced a rock physics model to discriminate pore pressure and saturation effect from time-lapse AVO reflection coefficients changes. It indicates the possibility of both positive and negative time-lapse reflection coefficients changes caused by fluid injection. To address this, we compute the local time shifts from the shallow (1000 ms) to the deep beneath the injection (2500 ms), shown in Figure 4. The positive time shift represents downward time shift of the post- from pre-injection datasets, vice versa. By comparing Figure 4 and Figure 3 (c),

we notice that the upward time shifts occurring from the shallow to the deep formation in the middle of Figure 4, which may cause the negative difference amplitudes within the injection interval, shown as the blue zone in Figure 3 (c). The near zero time shifts on both near sides may cause around zero amplitude differences within the injection interval at green zones in Figure 3 (c). The downward time shifts on both far sides in Figure 4 may relate to the positive difference amplitudes within the injection interval, as highlighted by orange zones in Figure 3 (c). Based on these data analysis, we reach the understanding that the polarity reversal character within the injection interval in Figure 3 (c) is most likely not caused by rock properties changes, but the misalignment between them. To separate the aliasing time shift from the time-lapse amplitude differences, we apply the registration method to the time-lapse datasets.

Well-log data and seismic well tie are presented in Figure 5, where the injection interval of lower Tuscaloosa Formation is highlighted as the yellow zone, appearing as permeable brine sand with lower velocity and density. The close tie between well-log synthetic and pre-injection seismic data allows us to apply the basis pursuit inversion later. The post injection data and the difference are aligned with the pre-injection data, where the difference does not contain any coherent features within the injection interval. It also shows that the injection interval is located between the trough and the zero cross of the seismic data with thickness of about 15 meters. A thin-bed may cause difficulty in delineating the CO_2 flow from the seismic amplitude, which could be improved by the inversion technique, such as the basis pursuit inversion method employed in this paper. The wavelet (Figure 6) is extracted from pre-injection data using calibration with well-log data and will be used for inversion of time-lapse datasets later.
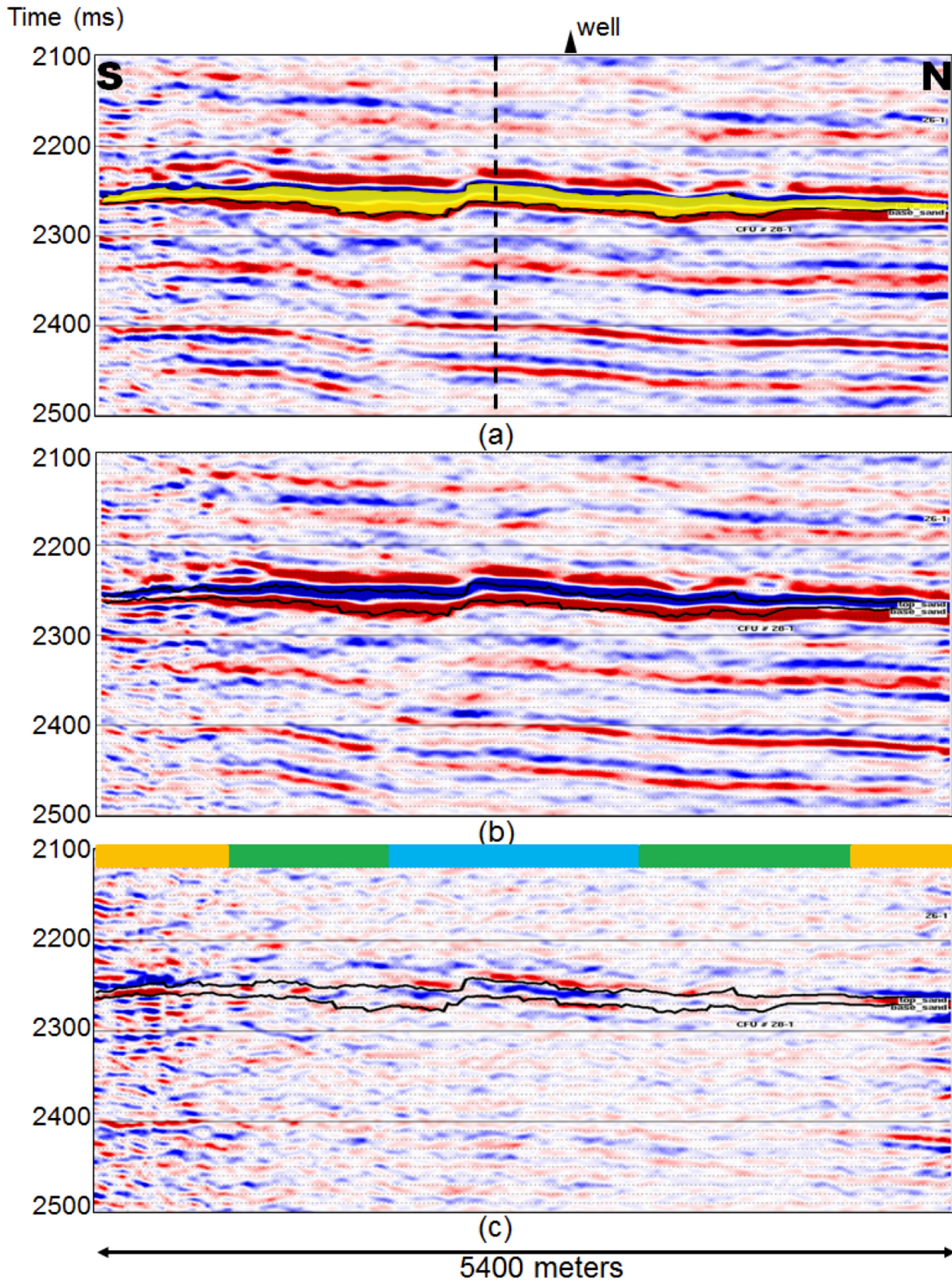
Figure 3. Cross-section of Time-lapse datasets of (a) pre-injection; (b) post-injection; and (c) their difference. The blue zone highlights the negative difference within the injection interval in the middle of the cross-section; green zones on both near sides highlight the near zero differences; and orange zones on both far sides highlight the positive difference within the injection interval.
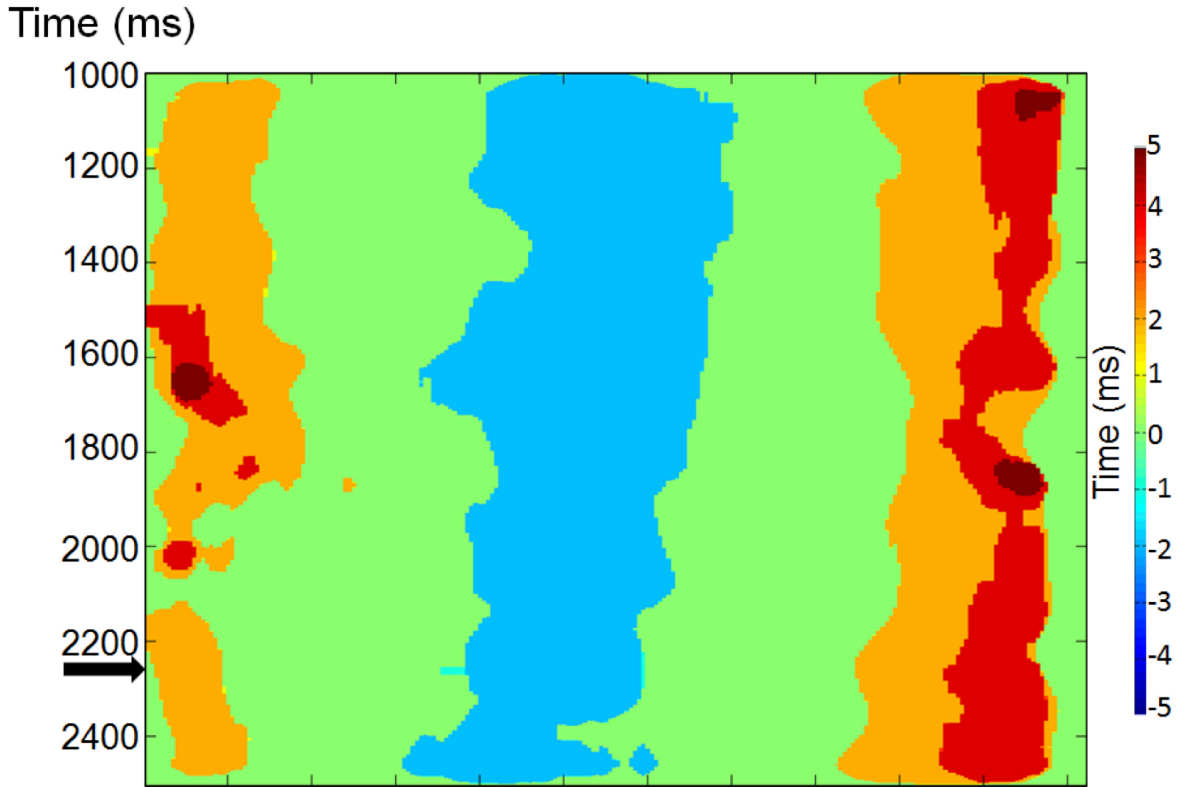
Figure 4. The local time shifts between the time-lapse datasets at the cross-section in Figure 3 from 1000 to 2500 ms. The injection interval is pointed by the black arrow.
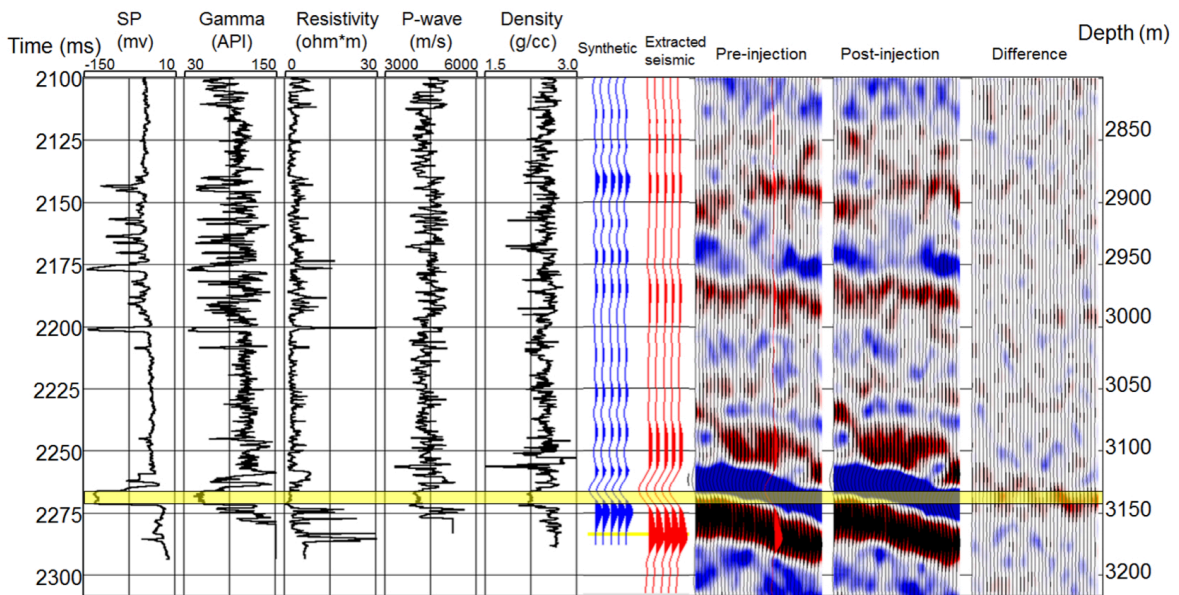

Figure 5. Well-logging, including SP, Gamma, Resistivity, Vp and density, is aligned with synthetic, extracted seismogram. Pre-, post- injection data and their difference closed to well location are shown in the right three panels.
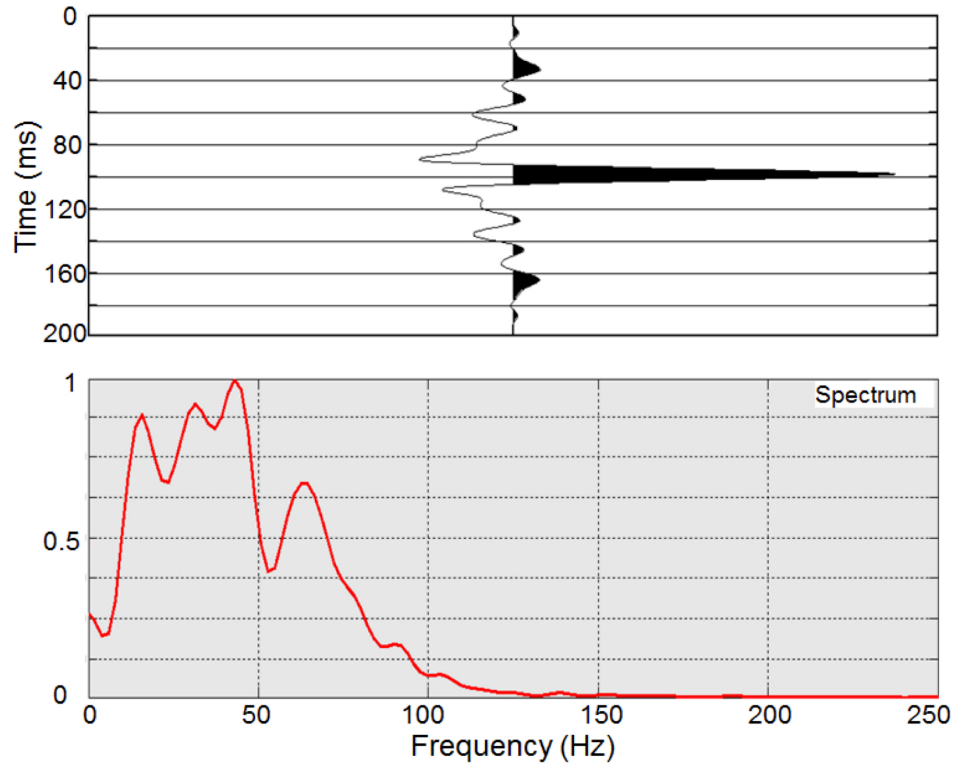
Figure 5. Extracted wavelet and its frequency spectrum.

METHODOLOGY

Time-lapse seismic data is aimed at monitoring the temporal changes of reservoir properties. The monitoring is mainly based on assessment of changes in seismic reflection amplitudes (e.g., Watts et al., 1996; Landrø et al., 1999). However, when the seismic data are acquired, processed through a multi-step workflow, the image can be contaminated at any step, which may be misinterpreted to be due to changes in fluid saturation. A registration method can help align the events and in turn, help in better identification of true time-lapse effects in seismic data. As discussed about in the previous section, CO_2 injection could result in both positive or negative reflection coefficients changes based on the combined pressure and saturation effects (Landrø, 2001). Besides, a coupled effect of velocity and thickness change can also cause positive or negative reflection coefficients changes (Ghaderi and Landrø, 2009). All of these rock properties change could be integrated with thin-bed tuning effect, which have been analyzed in some field cases (Jenkins et al., 1997, Guilbot and Smith, 2002, Arts and Vandeweijer, 2011). However, the polarity reversal within the injection interval at Cranfield shows considerable correlation with time shifts analysis from the shallow to the deep beneath the injection interval. Therefore, we apply a warping method based on local-correlation for the registration. The warping involves squeezing and stretching the monitor image according to the maximum local correlation trend

computed from the base and monitor datasets (Fomel and Jin, 2009). Thus, the warping does not change the amplitudes but shifts their locations. After the misalignment has been separated from the time-lapse datasets, the resulting time-lapse amplitude difference remains which could correctly represents the subsurface rock properties change caused by the CO_2 injection. To derive the rock properties change, we applied a basis pursuit inversion (BPI) for acoustic impedance on the time-lapse datasets after registration for acoustic impedance.

Local correlation

The conventional correlation between two discrete signals a_t and b_t is defined as:

$$c = \frac{\sum_t a_t b_t}{\sqrt{\sum_t a_t^2 \sum_t b_t^2}} \tag{1}$$

However, the cross-correlation produces one number that quantifies the global similarity between two vectors, which does not provide local similarity information. Hale (2006) introduced a local correlation method that measures the displacement from time-lapse seismic datasets. Hale (2009) later extended it to monitor the 7D displacement from 3D time-lapse datasets. Fomel (2007a) firstly developed a warping method based on the local correlation to register the PP and PS seismic data; and Fomel and Jin (2009) extended it to time-lapse data registration. The local correlation is derived by separating the Equation 1 as $c_t^2 = p_t q_t$ into two parts:

$$\mathbf{p}_t = \frac{\sum_t a_t b_t}{\sqrt{\sum_t b_t^2}} = (\mathbf{B}_t^T \mathbf{B}_t)^{-1} \mathbf{B}_t^T \mathbf{a}_t$$

$$\mathbf{q}_t = \frac{\sum_t a_t b_t}{\sqrt{\sum_t a_t^2}} = (\mathbf{A}_t^T \mathbf{A}_t)^{-1} \mathbf{A}_t^T \mathbf{b}_t \tag{2}$$

where A_t and B_t are two diagonal matrix with a_t and b_t as the diagonal elements. From the above equations, p_t and q_t can be considered as the least-square solutions for two minimization problems as:

$$\min_{p_t}\|\mathbf{a}_t - \mathbf{B}_t\mathbf{p}_t\|_2$$

$$\min_{q_t}\|\mathbf{b}_t - \mathbf{A}_t\mathbf{q}_t\|_2 .$$

(3)

Many kinds of regularization have been introduced by Tarantola (2004) for stabilization of inverse problems in equations 3. We use an iterative shaping regularization to control the smoothness of the solutions for the above equation 3 (Fomel, 2007b). In this paper, a_t and b_t are a pair of time-lapse seismic traces at the same location, which are normalized during the process of the local-correlation calculation.

Figure 7 shows a schematic example of the deviation of the relative stretch parameter γ. a_t is the base trace and b_t is the monitor trace. The monitor trace (b_t) is squeezed and stretched with γ ranging from 0.99 to 1.01 in the middle panel. A value of relative stretch parameter (γ) less than 1 means squeezing and larger than 1 means stretching the monitor trace. The local-correlation is calculated between the base and each squeezed or stretched monitor trace, resulting in a semblance-type panel called the local similarity scan (right panel in Figure 7). A trend of the maximum similarity is automatically picked (Fomel, 2009), which produces a warping parameter γ_t. The picked γ_t is then used for warping the monitor trace (Fomel and Jin, 2009; Kazemeini et al., 2010).
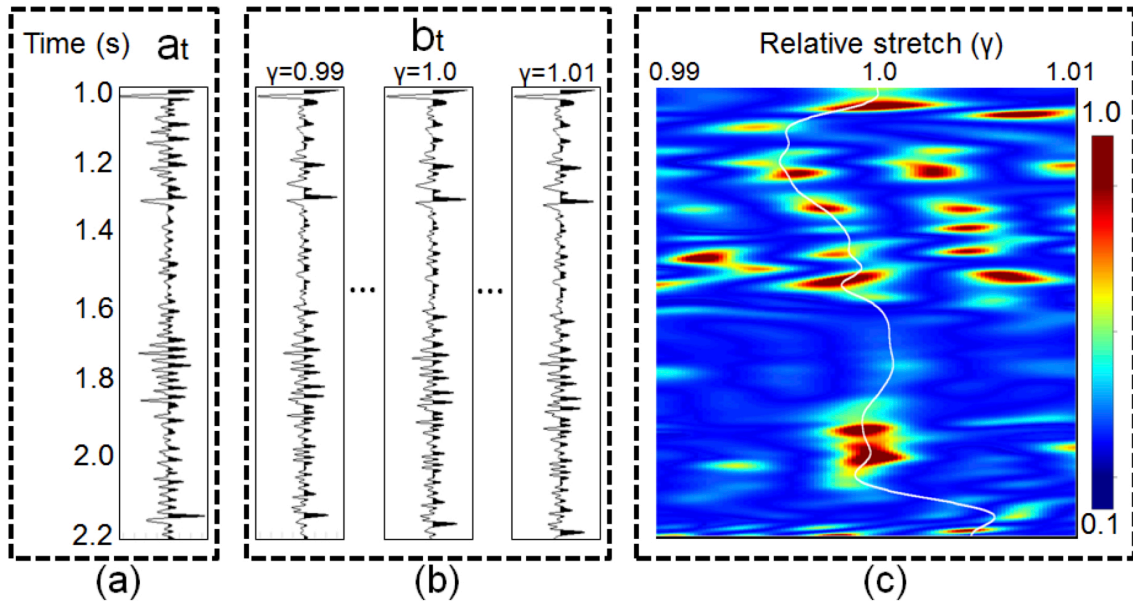

Figure 7. A schematic example of local-correlation derivation. a_t represents an example of a baseline trace; b_t with γ =1.0 represents a monitoring trace. The monitoring trace is stretched with relative stretch parameter γ ranging from 0.99 to 1.01. Ellipses represent the stretched results between them.

Warping

Warping was originally developed as spatial transformation of images for computer image manipulation and used extensively in animation and film special effects (e.g., Wolberg, 1994). Later developments of the original concept had been published mainly in computing and mathematical literature over the past few years (Modersitzki, 2009). This technique has been firstly implemented for imaging registration between different computed- tomography (CT) scan images (Thompson and Toga, 1997). Similar concepts relate to time-lapse seismic applications, i.e., the need for image matching and registration of time-lapse datasets to highlight changes that have occurred. Consequently, warping methodologies have been investigated for 4D seismic image registration in name of cross-equalization (Rickett and Lumley, 2001; Druzhinin and MacBeth, 2001; Nickel et al., 2003). The application of the warping on the time-lapse datasets at Cranfield consists of squeezing and stretching the post-injection data with respect to the derived relative stretched parameter γ_t.

Basis pursuit inversion

Basis pursuit inversion (BPI) was developed for improved resolution from original post- stack seismic data (Zhang and Castagna, 2011). It utilizes a L_1-norm optimization method within incorporating a wedge dictionary to approach high resolution. The objective function is shown in Equation 4, where **d** represents the seismic trace, **G** represents wavelet kernel matrix and **m** is reflection coefficients vector. Both least-squares error and L_1-norm of solution are minimized simultaneously with the weighting factor λ.

$$\min\left[\left\|\mathbf{d}-\mathbf{Gm}\right\|_2 + \lambda\left\|\mathbf{m}\right\|_1\right] \tag{4}$$

Unlike the conventional inversion method, BPI uses a wedge dictionary to construct a wavelet kernel matrix to approach thin-bed resolution. The procedure of BPI decompose each seismic trace based on wedge dictionary with corresponding decomposition coefficients and reconstruct the final thin bed reflectivity vector with the same decomposition coefficients. These high resolution refection coefficients can be converted into the acoustic impedance with incorporation of a low frequency initial model in a conventional way. The detailed information of BPI has been described by Zhang and Castagna (2011).

FIELD DATA APPLICATION

We firstly tested the registration on one trace from the previously shown cross-section (black dashed line in Figure 3 (a)). The original pre-, post- traces and their difference are shown in the Figure 8 (a). The difference is the subtraction of the pre- and post-injection traces. The semblance type local similarity scan (Figure 8 (b)) is derived in the same way as previously in Figure 7. The black dashed rectangles in Figures 8 (a) and (c) highlight the injection intervals. We find that the difference at shallow and deep parts becomes smaller after registration, as pointed by black arrows. Especially, the two strong sidelobes just above and below the injection interval have been suppressed after registration, as indicated by the red arrows. The local similarity scan after warping (Figure 8 (d)) shows that the maximum correlation trend is more centered around 1 compared to Figure 8 (b). This behavior demonstrates the effectiveness of the registration and gives us confidence to apply it to 2D and 3D datasets.
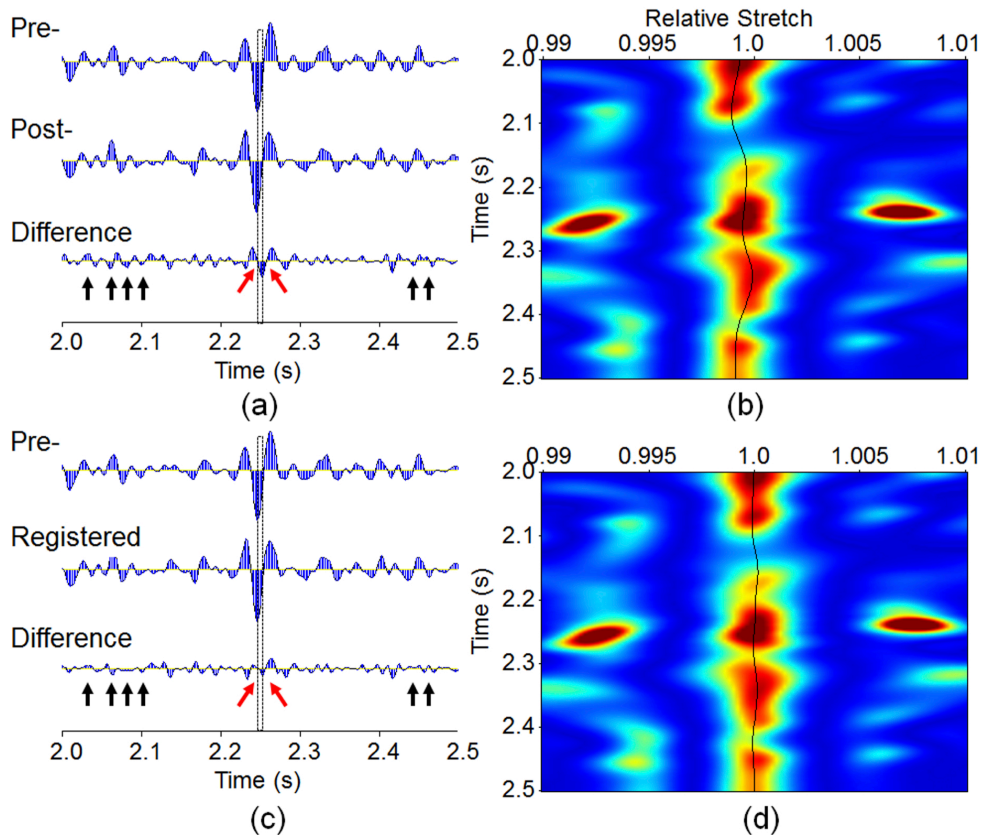

Figure 8. (a) shows the time-lapse traces and their difference; (b) shows the semblance type local similarity scan and the picked trend; (c) and (d) show the warped post-injection and the local similarity scan again.

We applied the registration on the 2D cross-section in Figure 3 in a trace by trace manner. The local similarity scan between the original time-lapse datasets is shown in Figure 9 (a), and Figure 9 (b) shows the 2D picked relative stretch parameter. Figure 9 (c) shows the local similarity scan after registration with the maximum local correlation more centered around 1. The post-injection data after registration is shown in Figure 10 (b) and its difference from original pre-injection data (Figure 10 (a)) is shown in Figure 10 (c). The registered difference (Figure 10 (c)) contains strong laterally continuous negative amplitude (blue) within the injection interval, which is noticeably different from the original time-lapse difference (Figure 3 (c)). Such laterally continuous amplitude behavior here could imply a possible CO_2 effect of the acoustic impedance drop occurring within the injection interval. However, we also notice an anomalous misalignment induced by the registration, as shown within the ellipse area in Figure 10 (b).
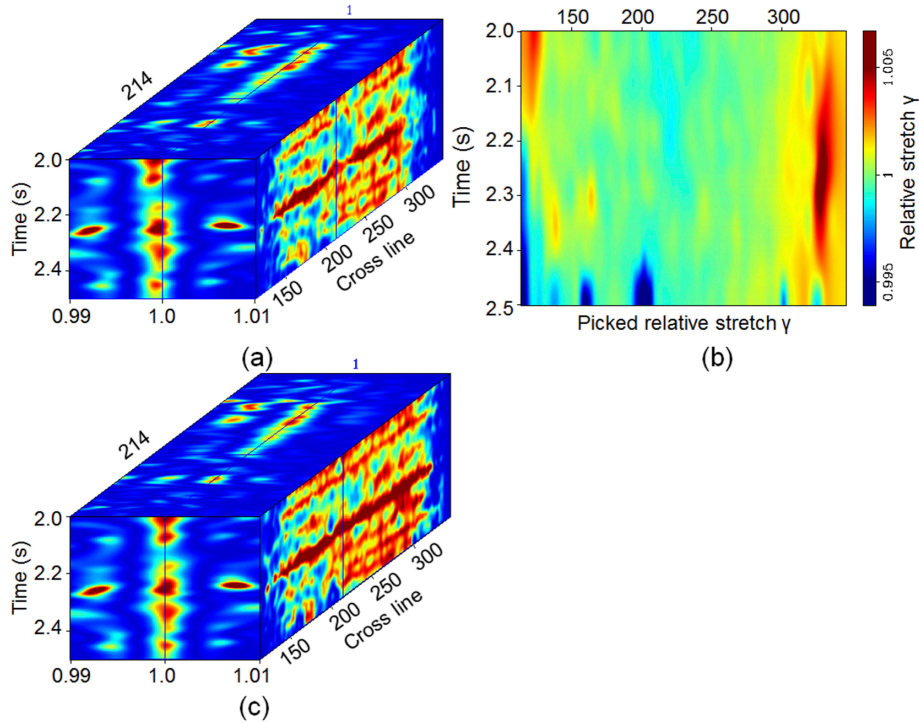

Figure 9. 2D local similarity scan of time-lapse cross-section in Figure 3. (a) shows local similarity scan before registration; (b) shows 2D maximum local similarity picking from (a); (c) shows local similarity scan after registration.

The original time-lapse seismic amplitudes and their differences are extracted at the top of the injection interval, as shown in Figures 11 (a), (b) and (d). Because the registration does not change anything of pre-injection data, the post-injection data slice after registration is shown in Figures 11 (c). Figure 11 (e) shows the difference from pre-injection data after registration. Figures 11 (a), (b) and (c) are plotted in the same normalized color scale from -3.0 to 0.5; while Figures 11 (d) and (e) are plotted in another same normalized color scale from -1.0 to 1.0. The

red color in Figures 11 (d) and (e) representing positive value means decreases from pre- to post-injection data, vice versa. It is obvious that the top horizon slice mostly shows up as negative amplitude, as shown in Figure 11 (a), (b) and (c). The original time-lapse difference at top slice in Figure 11 (d) shows a smear distribution of positive values covering most of area, which is hard to delineate local CO_2 injection effect. However, the top difference slice after registration (Figure 11 (e)) shows more patchy distribution of positive values, which have been circled out separately with black dashed lines. Such localized distribution can be more helpful to calibrate with local CO_2 injection activities. We notice that these circled areas also show as positive values before registration, except an area changing from positive to negative values, as circled by blue dashed line in Figure 11 (e) and pointed by blue arrows in Figure 11 (d). This could lead to the disregard of this area out of the CO_2 plume.

Next we applied the Basis pursuit inversion (BPI) for acoustic impedance to both preinjection and warped post-injection datasets (Figure 12) using the same wavelet (Figure 6). The $L1$-norm optimization and the wedge dictionary incorporated with the BPI result in the blocky shape of the output acoustic impedance with improved resolution comparing the original seismic data (Zhang and Castagna, 2011). The blocky acoustic impedances (Figure 12 (a) and (b)) contain sharp boundaries at layer interfaces which visualize the injection interval clearly. This block characteristic shows an important advantage for the timelapse impedances comparison because two impedances have sharp boundaries at the same locations while inner layer values could represent the time-lapse effects. The impedance difference is calculated by subtracting the post- from pre- injection acoustic impedances as shown in Figure 12 (c). The blue color represents positive value, which means decrease from pre- to post- injection datasets. Figure 13 shows a detailed view of the inverted impedances and their difference. We find from the impedance difference (Figure 13 (c)) that a strong impedance decrease occurs at the top of the injection interval. This finding agrees with the well-log measurements that the injected CO_2 mostly accumulates at the top of the injection interval. In addition, these impedances could be used to map out the CO_2 plume in future.
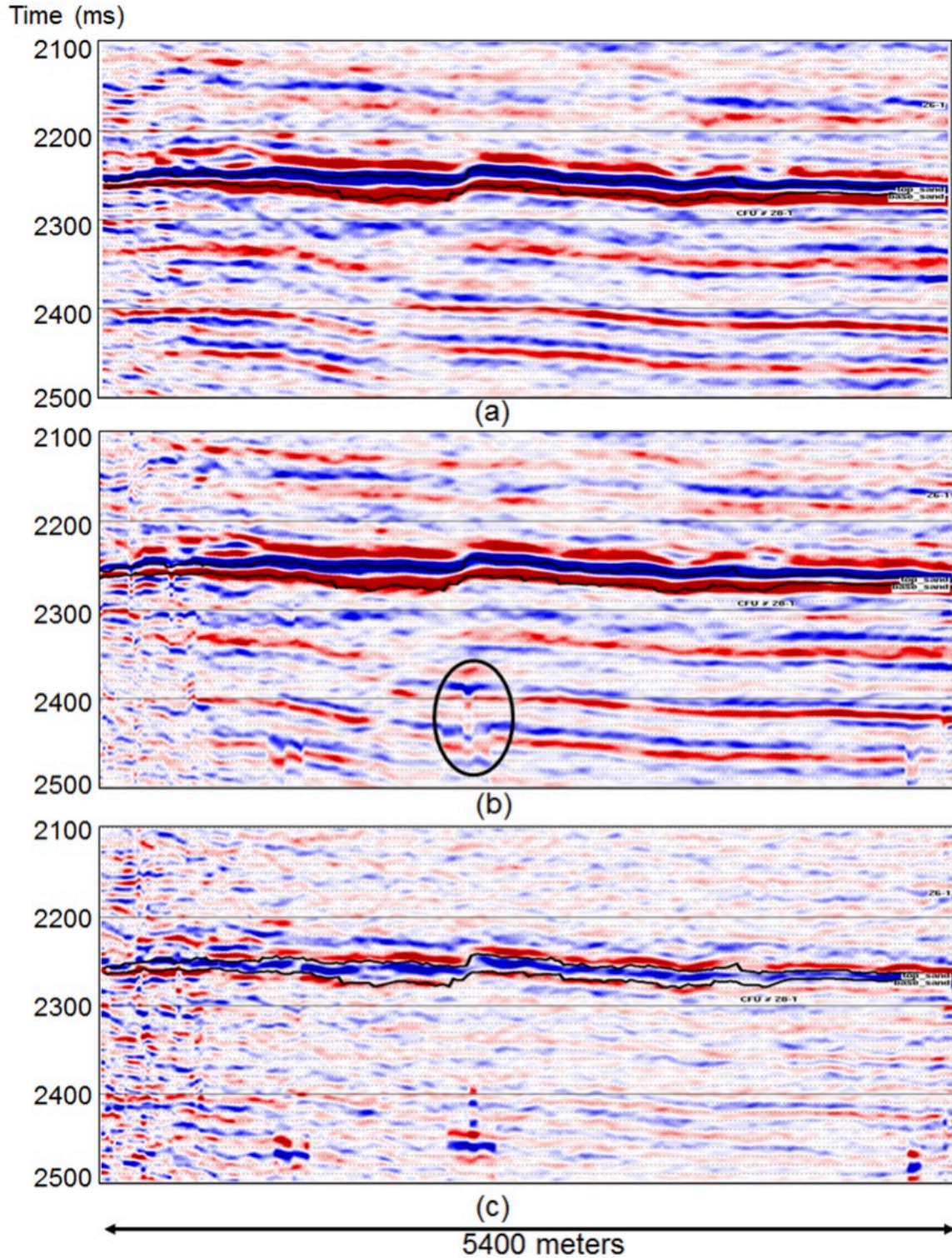
Figure 10. (a) shows the original pre-injection data; (b) shows the post-injection data after registration; and (c) shows their difference.
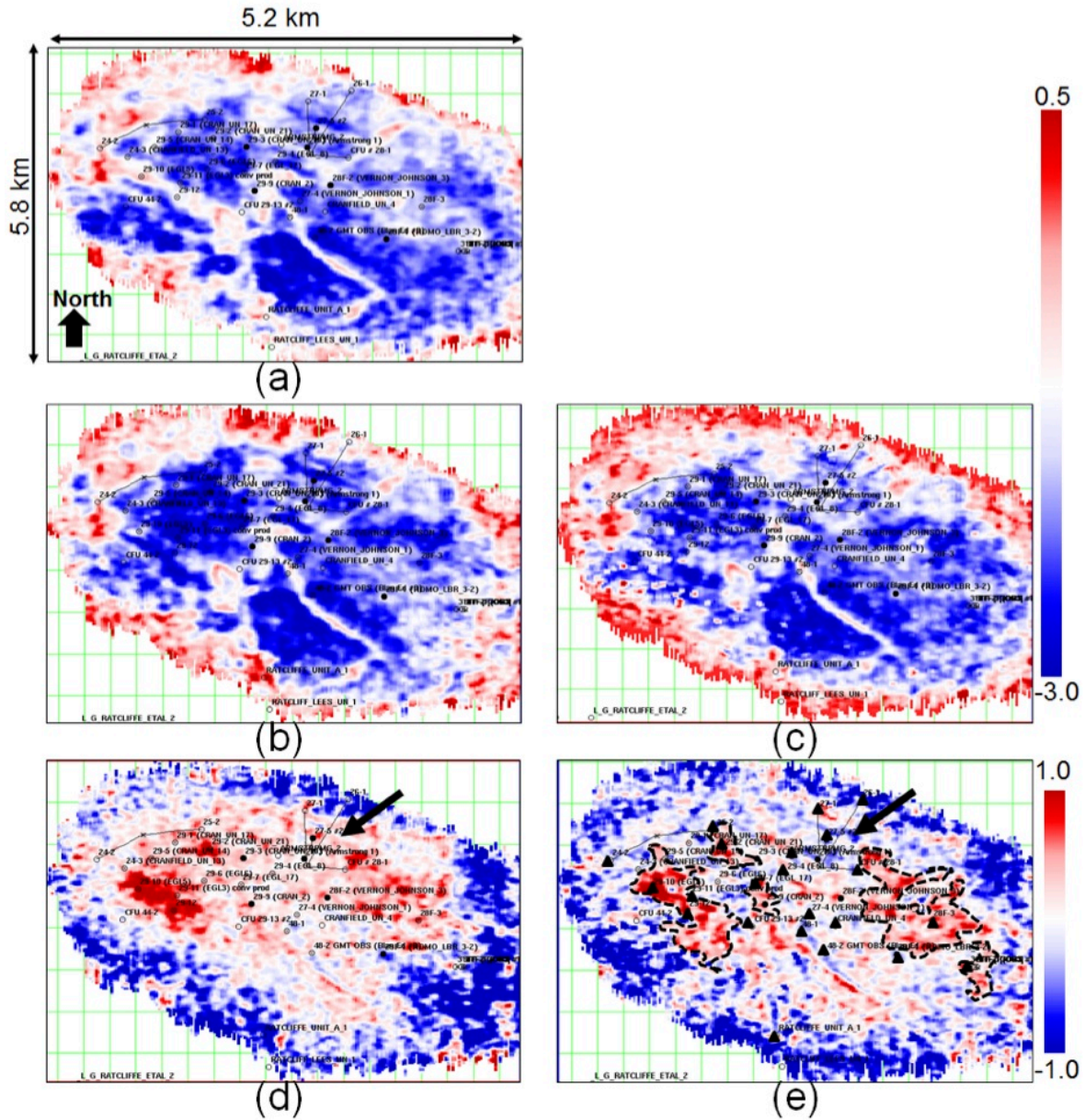
Figure 11. Time-lapse seismic amplitudes and their difference slices are extracted at the top of the injection interval. (a) shows the pre-injection amplitude slice; (b) and (c) show the post-injection amplitude slices before and after registration; (d) and (e) show the time-lapse difference slices before and after registration.
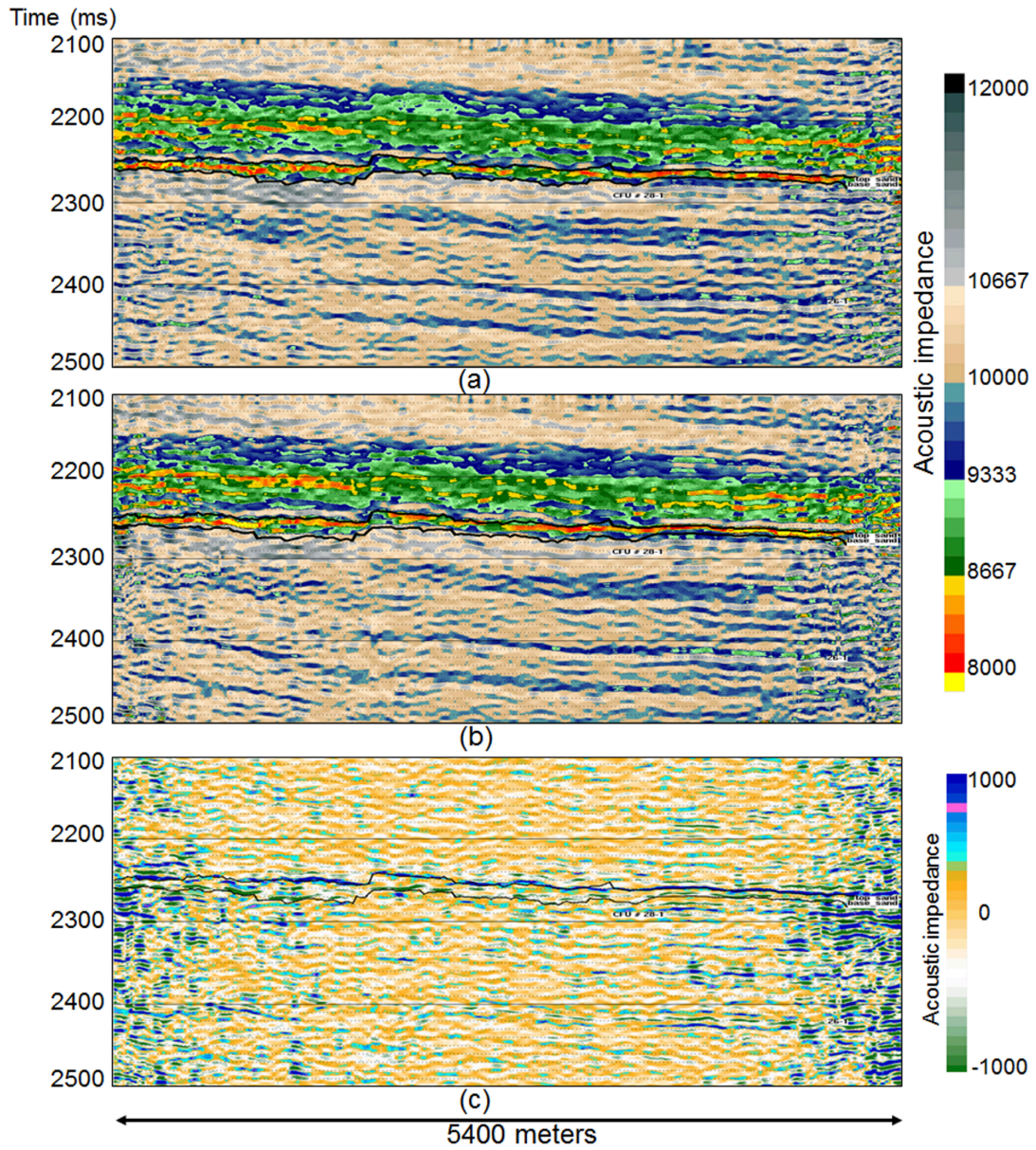
Figure 12. (a) and (b) show the acoustic impedances from the pre-injection and warped post-injection datasets. (c) shows the difference between them.
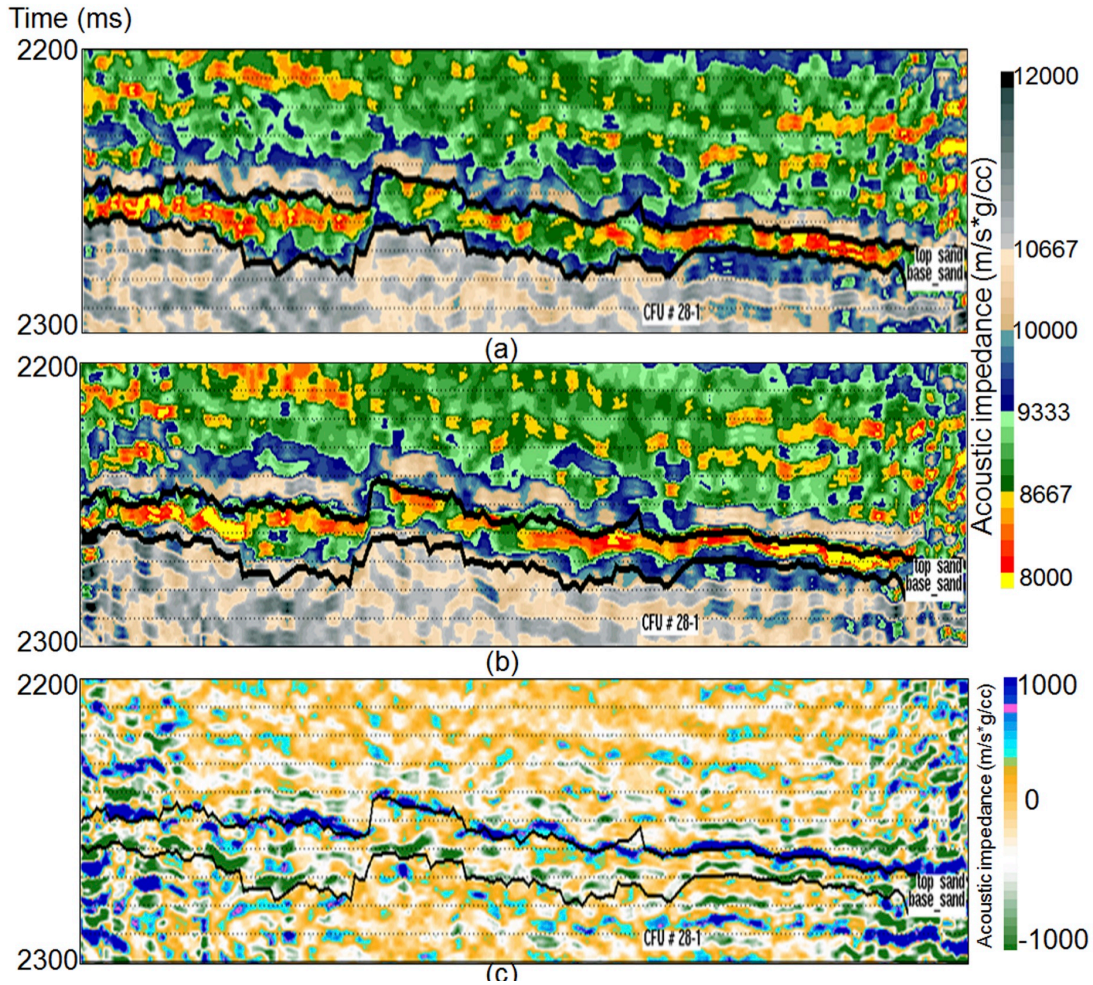
Figure 13. (a) and (b) show the acoustic impedances from the pre-injection and warped post-injection datasets. (c) shows the difference between them.

DISCUSSIONS

The time-shift between time-lapse seismic datasets has been utilized as a real time-lapse attribute caused by the fluid movements in many studies. In this paper, examination of the time-lapse datasets at Cranfield shows that the reversal amplitude differences within the injection interval (Figure 3 (c)) and the nearly constant time shifts from the shallow to the deep formation (Figure 4) appear similar lateral distribution. This leads to our assumption that the time shifts between time-lapse datasets is an aliasing artifact for this case, which needs to be corrected. The differences after registration show as the laterally continuous negative amplitudes within the injection interval in cross-section (Figure 10 (c)) and more localized distribution in horizon slices (Figure 11 (e)). However, the recognition of the aliasing time shift at Cranfield datasets is based on the knowledge of regional geology and careful analysis of the time-lapse datasets, we suggest very careful analysis and study when considering other datasets.

The local-correlation method provides a way to evaluate the localized similarity, which shows obvious advantage over the global correlation. By scanning the similarity between the time-lapse datasets, a semblance type similarity image can be constructed as shown in Figures 8 (b) and (d). The maximum similarity trend, which is interpreted as relative stretch parameter for the warping operation, can be centralized around 1 after registration. The local-correlation derivation relies on the inversion solution (equation 3) with shaping regularization (Fomel, 2007b). The proper regularization parameters to adopt can be obtained from a single trace test, as in Figure 8.

Basis pursuit inversion can provide acoustic impedance with improved resolution, as shown in Figures 12 and Figure 13. The inverted impedances highlight the injection interval clearly with sharp boundaries at the top and base of the injection interval. Thanks to the registration, the time-lapse impedances have the layer boundaries located at the same places. The impedance difference could reliably reflect the impedance changes within the injection interval without any misalignment. This difference can also be used for mapping the CO_2 plume, and furthermore, estimation of the CO_2 saturation.

CONCLUSIONS

Time shifts between time-lapse seismic datasets at Cranfield have been tested and recognized as an aliasing. To correct this, we apply the registration method on the time-lapse datasets to enhance the apparent alignment. The improved alignment between the datasets after registration results in the laterally continuous amplitude differences within the injection interval and more localized distribution of CO_2 effect in horizon slices. The improved consistence between time-lapse datasets also allows us to apply the basis pursuit inversion on the time-lapse datasets for the blocky acoustic impedances. Because of the registration, the time-lapse impedances, also appearing good consistence, show decreases after CO_2 injection mostly occurring at the top of the injection interval. All of these results can be integrated to estimate the spatial distribution of the CO_2 plume effectively.

ACKNOWLEDGEMENTS

REFERENCES

Arts, R., and V. Vandeweijer, 2011, The challenges of monitoring storage: The Leading Edge, **30**, 1026–1033.

Buland, A., and Y. E. Ouair, 2006, Bayesian time-lapse inversion: Geophysics, **71**, R43–R48.

Burkhart, T., A. R. Hoover, and P. B. Flemings, 2000, Time-lapse (4-D) seismic monitoring of primary production of turbidite reservoirs at South Timbalier Block 295, offshore Louisiana, Gulf of Mexico: Geophysics, **65**, 351–367.

Calvert, R., 2005, 4D technology: where are we, and where are we going?: Geophysical Prospecting, **53**, 161–171.

Druzhinin, A., and C. MacBeth, 2001, Robust cross-equalization of 4D-4C PZ migrated data at Teal South: SEG Technical Program Expanded Abstracts, **20**, 1670–1673.

Falahat, R., A. Shams, and C. MacBeth, 2011, Towards quantitative evaluation of gas injection using time-lapse seismic data: Geophysical Prospecting, **59**, 310–322.

Fomel, S., 2007a, Local seismic attributes: Geophysics, **72**, A29–A33.

——, 2007b, Shaping regularization in geophysical-estimation problems: Geophysics, **72**, R29–R36.

——, 2009, Velocity analysis using AB semblance: Geophysical Prospecting, **57**, 311–321.

Fomel, S., and L. Jin, 2009, Time-lapse image registration using the local similarity attribute: Geophysics, **74**, A7–A11.

Ghaderi, A., and M. Landrø, 2009, Estimation of thickness and velocity changes of injected carbon dioxide layers from prestack time-lapse seismic data: GEOPHYSICS, **74**, O17–O28.

Guilbot, J., and B. Smith, 2002, 4-D constrained depth conversion for reservoir compaction estimation: Application to Ekofisk Field: The Leading Edge, **21**, 302–308.

Hale, D., 2006, Fast local cross-correlations of images: SEG Technical Program Expanded Abstracts, **25**, 3160–3164.

——, 2009, A method for estimating apparent displacement vectors from time-lapse seismic images: Geophysics, **74**, V99–V107.

Hall, S. A., 2006, A methodology for 7D warping and deformation monitoring using time lapse seismic data: Geophysics, **71**, O21–O31.

Hall, S. A., C. MacBeth, O. I. Barkved, and P. Wild, 2005, Cross-matching with interpreted warping of 3D streamer and 3D ocean-bottom-cable data at Valhall for time-lapse assessment: Geophysical Prospecting, **53**, 283–297.

Hall, S. A., C. MacBeth, J. Stammeijer, and M. Omerod, 2006, Time-lapse seismic analysis of pressure depletion in the Southern Gas Basin: Geophysical Prospecting, **54**, 63–73.

Hersch, J. B., 1987, Exploration methods-lower Tuscaloosa trend, Southwest Mississippi: Gulf Coast Association of Geological Societies Transactions, **37**, 105–112.

Hovorka, S. D., T. A. Meckel, R. H. Trevino, J. Lu, J.-P. Nicot, J.-W. Choi, D. Freeman, P. Cook, T. M. Daley, J. B. Ajo-Franklin, B. M. Freifeild, C. Doughty, C. R. Carrigan, D. L. Brecque, Y. K. Kharaka, J. J. Thordsen, T. J. Phelps, C. Yang, K. D. Romanak, T. Zhang, R. M. Holt, J. S. Lindler, and R. J. Butsch, 2011, Monitoring a large volume CO_2 injection: Year two results from SECARB project at Denbury LLC Cranfield, Mississippi, USA: Energy Procedia, **4**, 3478 – 3485. (10th International Conference on Greenhouse Gas Control Technologies).

Isaac, J. H., and D. C. Lawton, 2006, A case history of time-lapse 3D seismic surveys at Cold Lake, Alberta, Canada: Geophysics, **71**, B93–B99.

Jenkins, S., M. Waite, and M. Bee, 1997, Time-lapse monitoring of the Duri steamflood: A pilot and case study: The Leading Edge, **16**, 1267–1274.

Kazemeini, S. H., C. Juhlin, and S. Fomel, 2010, Monitoring CO_2 response on surface seismic data; a rock physics and seismic modeling feasibility study at the CO_2 sequestration site, Ketzin, Germany: Journal of Applied Geophysics, **71**, 109 – 124.

Klicman, D. P., C. P. Cameron, and M. A. Meylan, 1988, Petrology and Depositional Environments of Lower Tuscaloosa Formation (Upper Cretaceous) Sandstones in the North Hustler and Thompson Field Areas, Southwest Mississippi: Gulf Coast Association of Geological Societies Transactions, **38**, 47–58.

Landrø, M., 2001, Discrimination between pressure and fluid saturation changes from time lapse seismic data: GEOPHYSICS, **66**, 836–844.

——, 2002, Uncertainties in quantitative time-lapse seismic analysis: Geophysical Prospecting, **50**, 527–538.

Landrø, M., O. A. Solheim, E. Hilde, B. O. Ekren, and L. K. Stronen, 1999, The Gullfaks 4D seismic study: Petroleum Geoscience, **5**, 213–226.

Lumley, D., 2001, Time-lapse seismic reservoir monitoring: Geophysics, **66**, 50–53.

MacBeth, C., M. Floricich, and J. Soldo, 2006, Going quantitative with 4D seismic analysis: Geophysical Prospecting, **54**, 303–317.

Meckel, T., and S. Hovorka, 2009, A new generation of seismic navigation calibration techniques: SPE International Conference on CO_2 Capture, Storage, and Utilization, 2-4 November 2009, San Diego, California, USA, Society of Petroleum Engineer, 1–3. Mississippi Oil Gas Board, 1966, Cranfield Field, Cranfield unit, Basal Tuscaloosa reservoir, Adams and Franklin Counties, Mississippi: 42–58.

Modersitzki, J., 2009, FAIR: Flexible algorithms for image registration: SIAM. Nickel, M., J. Schlaf, and L. Sønneland, 2003, New tools for 4D seismic analysis in compacting reservoirs: Petroleum Geoscience, **9**, 53–59.

Reid, F. J., A. Bertrand, A. T. McInally, and C. MacBeth, 2005, 4D signal enhancement using singular-value decomposition: application to mapping oilwater contact movement across the Nelson Field: Geophysical Prospecting, **53**, 253–263.

Rickett, J. E., and D. E. Lumley, 2001, Cross-equalization data processing for time-lapse seismic reservoir monitoring: A case study from the Gulf of Mexico: Geophysics, **66**, 1015–1025.

Spooner, H. V., 1964, Basal Tuscaloosa sediments, east-central Louisiana: AAPG Bulletin, **48**, 1–21.

Staples, R., P. Hague, T. Weisenborn, P. Ashton, and B. Michalek, 2005, 4D seismic for oil-rim monitoring: Geophysical Prospecting, **53**, 243–251.

Tarantola, A., 2004, Inverse problem theory.

Thompson, P. M., and A. W. Toga, 1997, Detection, visualization and animation of abnormal anatomic structure with a deformable probabilistic brain atlas based on random vector field transformations: Medical Image Analysis, **1**, 271–294.

Vedanti, N., and M. K. Sen, 2009, Seismic inversion tracks in situ combustion: A case study from balol oil field, india: Geophysics, **74**, B103–B112.

Wagner, S. R., W. D. Pennington, and C. MacBeth, 2006, Gas saturation prediction and effect of low frequencies on acoustic impedance images at Foinaven Field: Geophysical Prospecting, **54**, 75–87.

Watts, G. F. T., D. Jizba, D. E. Gawith, and P. Gutteridge, 1996, Reservoir monitoring of the magnus field through 4D time-lapse seismic analysis: Petroleum Geoscience, **2**, 361–372.

Wolberg, G., 1994, Digital image warping, 1st ed.: IEEE Computer Society Press.

Womack, R., 1950, Brookhaven oil field, Lincoln County, Mississippi: AAPG Bulletin, **34**, 1517–1529.

Zhang, R., and J. Castagna, 2011, Seismic sparse-layer reflectivity inversion using basis pursuit decomposition: Geophysics, **76**, R147–R158.

Zhang, R., R. Ghosh, M. K. Sen, and S. Srinivasan, 2012, Time-lapse surface seismic inversion with thin bed resolution for monitoring CO_2 sequestration: A case study from Cranfield, Mississippi: International Journal of Greenhouse Gas Control, –.